Available online at www.sciencedirect.com
ScienceDirect
Applied Catalysis B: Environmental 78 (2008) 288–300
APPLIED CATALYSIS B: ENVIRONMENTAL
www.elsevier.com/locate/apcatb

Comparative study of structural properties and NO_x storage-reduction behavior of $Pt/Ba/CeO_2$ and $Pt/Ba/Al_2O_3$

M. Casapu [a], J.-D. Grunwaldt [a,*], M. Maciejewski [a], F. Krumeich [a], A. Baiker [a,*], M. Wittrock [b], S. Eckhoff [b]

[a] *Institute for Chemical and Bioengineering, Department of Chemistry and Applied Biosciences, ETH Zurich, Hönggerberg, CH-8093 Zürich, Switzerland*
[b] *Umicore AG & Co. KG, Rodenbacher Chaussee 4, D-63403 Hanau-Wolfgang, Germany*

Received 21 August 2007; received in revised form 21 September 2007; accepted 24 September 2007
Available online 29 September 2007

Abstract

Differences in the NO_x storage-reduction (NSR) behavior of $Pt/Ba/CeO_2$ and $Pt/Ba/Al_2O_3$ have been identified and traced to their different chemical and structural properties. The results show that $Pt/Ba/CeO_2$ exhibits inferior NO_x storage and, particularly, reduction (regeneration) activity compared to the Al_2O_3 supported catalyst. The incomplete reduction of the stored NO_x-species in $Pt/Ba/CeO_2$ seems to be caused by a faster and more profound reoxidation of Pt particles during the lean period as evidenced by *in situ* X-ray absorption spectroscopy. Interestingly, the reduction activity could be significantly improved by a pre-reduction step at mild conditions. Exposure of the $Pt/Ba/CeO_2$ catalyst to reducing H_2 atmosphere in the temperature range 300–500 °C lead to a moderate increase of Pt particle size which beneficially influenced the regeneration activity. In contrast, pre-reduction at temperatures above 500 °C was unfavorable and resulted in a severe decrease of the regeneration activity, probably due to migration of the partially reduced CeO_2 onto the surface of Pt particles.

Keywords: NO_x storage-reduction catalyst; Ceria; Pre-treatment; Thermal analysis; X-ray absorption spectroscopy

1. Introduction

Ceria is a widely used material in exhaust gas catalysis but has only recently been used in the field of NO_x storage-reduction catalysts. The common application of CeO_2 in three-way automotive catalysis results from the fact that ceria can act as an oxygen-storage component [1–4]. Due to the high mobility of the lattice oxygen, it buffers the composition of the exhaust gas around the stoichiometric point during cyclic lean-rich fluctuations by providing oxygen for oxidizing CO and hydrocarbons (fuel rich conditions) and removing it from the exhaust gas phase for reducing NO_x (lean conditions). Moreover, several other functions of ceria appear beneficial, such as: promoting water–gas shift (WGS) and steam reforming reactions [5–7], enhancing dispersion of the metals [8,9], stabilizing sintering of alumina [10,11], and promoting CO oxidation activity [12]. Ceria is also utilized to catalyze the oxidation of soot with NO_2 [13,14]. Thus, the effectiveness of CeO_2 goes much beyond three-way catalysts and it appears an interesting material also for other areas.

Although in NO_x storage-reduction (NSR) catalysis several studies have examined the effect of CeO_2 addition as promoter, only a few investigations deal directly with the use of CeO_2 as support for the storage component (Ba, K) and the noble metal (Pt, Rh). This concerns particularly the NO_x storage capacity of CeO_2 containing materials [15–18], whereas its influence on the NO_x storage-reduction activity has only been reported by a few research groups [19–21]. Liotta et al. [19] found comparable performances of Pt supported CeO_2–ZrO_2/BaO–Al_2O_3 to those of Pt/BaO–Al_2O_3 and explained this behavior by the better dispersion of Ba species in the CeO_2–ZrO_2 containing catalyst. Theis et al. [20] studied the effect of the ceria content on the performance of the NO_x storage-reduction catalysts. They showed that the time required for catalyst regeneration and the amount of NO_x released increased at higher ceria content.

* Corresponding author. Fax: +41 1 632 11 63.
E-mail addresses: grunwaldt@chem.ethz.ch (J.D. Grunwaldt), baiker@chem.ethz.ch (A. Baiker).

0926-3373/$ – see front matter © 2007 Elsevier B.V. All rights reserved.
doi:10.1016/j.apcatb.2007.09.030

Nevertheless, they observed that the sulfur tolerance and NO_x conversion after ageing were improved by addition of ceria. Investigating the influence of supporting material and Ba-loading on the NO_x storage, stability of stored NO_x species and their reduction, Piacentini et al. [21] found recently that Pt/Ba/CeO_2 catalysts show at Ba-loadings up to ca. 10% a higher NO_x storage capacity than corresponding zirconia-, alumina- and silica-supported catalysts. They correlate this behavior with the higher storage contribution of ceria support. In our former studies on the ageing phenomena occurring in Pt/Ba/CeO_2 and Pt/Ba/Al_2O_3 we proposed a method for the reactivation of CeO_2 aged catalysts using some gaseous components present in the exhaust gases [22–24]. Therefore, there are several reasons indicating that CeO_2 could be an interesting support for NO_x storage-reduction catalysts.

Here we compare the structural properties and NO_x storage-reduction behavior of Pt/Ba/CeO_2 to those of a corresponding Pt/Ba/Al_2O_3 reference catalyst. Based on this study a pre-treatment process is elaborated that improves the NSR-properties of CeO_2 supported catalysts.

2. Experimental part

2.1. Sample preparation

Pt/Ba/Al_2O_3 and Pt/Ba/CeO_2 model catalysts with the principal composition: Pt(1 g)/Ba(20 g)/γ-Al_2O_3(100 g) and Pt(1 g)/Ba(20 g)/CeO_2(100 g) were prepared by incipient wetness impregnation of the commercial γ-alumina and ceria (Umicore) as described in a previous paper [22]. In brief, at first the support was impregnated with an aqueous solution of dinitrodiamine platinum (Strem Chemicals). In a second step, Ba species were added using aqueous solution of barium acetate (Fluka). After every impregnation the samples were dried over night at 80 °C and then calcined in air at 500 °C for 5 h. These catalysts were denoted as Pt/Ba/support. In the case of ceria-supported catalysts two other Pt/Ba/CeO_2 samples were prepared by changing the order of the impregnation steps (first Ba and then Pt species were added) and the Pt loading: Pt(1 g)-top/Ba(20 g)/CeO_2(100 g), denoted as Pt(1)-top/Ba/CeO_2 and Pt(4 g)-top/Ba(20 g)/CeO_2(100 g), denoted as Pt(4)-top/Ba/CeO_2. Additionally Pt(4 g)/CeO_2(100 g), Pt(10 g)/CeO_2(100 g) and Pt(10 g)/Al_2O_3(100 g) samples were prepared by the same method and denoted 4-Pt/CeO_2 and 10-Pt/support.

2.2. Characterization techniques

X-ray diffraction measurements were carried out on a Siemens D5000 powder X-ray diffractometer using the Cu Kα radiation, in the step scanning mode between $2\Theta = 15^\circ$ and 65°, with a step size of 0.01° and 2 s per step. The intensities of the reflections were calibrated by comparison with the internal standard, i.e. the intensity of Cu(1 1 1) reflection at $2\theta = 43.18^\circ$.

Thermal analysis (TA and PulseTA [25]) experiments were performed on a Netzsch STA 409 thermoanalyser equipped with a pulse device enabling injection of a certain amount of one or two pure gases or gaseous mixtures into the carrier gas stream flowing through the system. The flow rate was controlled by mass flow controllers (Brooks model 5850E). The outlet of the thermoanalyser was connected by a heated (ca. 150 °C) stainless steel capillary to a mass spectrometer for gas analysis (Pfeiffer Vacuum OmniStar).

The temperature programmed reaction experiments were carried out in an inert atmosphere (He) using ca. 70 mg samples. Prior to each experiment the samples were heated up to 500 °C with a heating rate of 10 °C/min for removal of all physisorbed species. NO_x storage-reduction tests were performed at 300 °C. The NO_x storage step was simulated using 1 ml O_2 and NO pulses (3 ml O_2 and 2 ml NO in each cycle) injected into the carrier gas stream of 50 ml/min. The regeneration of the catalyst was done with 1 ml pulses of C_3H_6.

The BET surface area and pore size distribution were determined on a Tristar (micrometrics Instruments) by N_2 adsorption–desorption measurements. Before the measurement the samples were degassed in vacuum at 150 °C.

X-ray photoelectron spectroscopy (*XPS*). A Leybold Heraeus LHS 11 MCD XPS apparatus was used to determine the surface composition of the catalysts. The photoelectrons were exited with Mg Kα radiation and further analysed with the analyser operated at 150 eV pass energy. The energy scale was calibrated versus C 1 s at 289.4 eV. The surface composition of the samples was determined from the peak areas of the corresponding lines using a Shirley type background and empirical cross-section factors for XPS [26].

XANES and EXAFS experiments were performed at the beamline X1 at HASYLAB in Hamburg, Germany. The storage ring typically operated at 4.45 GeV with an injection current of 140 mA. A Si(1 1 1) double-crystal was used as monochromator. The higher harmonics were removed by detuning crystals to 60% of the maximum intensity. EXAFS data were collected in the fluorescence and transmission mode using an *in situ* cell with X-ray fluorescence and transmitting windows. A five-element Ge solid-state detector was used to measure the fluorescence X-rays of the element of interest. Spectra were taken around the Pt L_3-edge (11.564 keV), using a Pt foil as reference for energy calibration. For the *in situ* fluorescence measurements the sample was placed in a 45° angle both to the beam and the detector. The outlet of the cell was connected to a mass spectrometer (Pfeiffer Vacuum Omnistar). For data evaluation the WINXAS 3.1 software was used [27]. Additional measurements at Pt L_3-edge were performed at the Swiss-Norwegian beamline (SNBL) at the European Synchrotron Radiation Facility (ESRF) in Grenoble, France. The electron energy was 6.0 GeV and the maximum ring current was 200 mA. A Si(1 1 1) crystal was used as monochromator. EXAFS data were collected in the fluorescence mode at room temperature.

Electron microscopy. The transmission electron microscopy (TEM), scanning transmission electron microscopy (STEM) and energy dispersive X-ray (EDX) investigations were performed on a Tecnai F30 microscope. Crushed samples were suspended in ethanol and deposited on a holey carbon foil supported on a copper grid. TEM images were recorded with a slow-scan CCD camera. The energy-dispersive X-ray spectrometer attached to the Tecnai F30 allowed also the elemental

analyses at spots selected in the high-angle annular dark field (HAADF-STEM) images.

CO-pulse chemisorption measurements were used to determine the dispersion of Pt. The measurements were performed on a Micrometrics Autochem II 2920 unit at 45 °C using a He flow of 20 ml/min and pulses of 0.5 ml (10% CO in He). Prior to analysis all samples were reduced for 1 h at selected temperatures using pure H_2 (20 ml/min) and then flushed with He for 1 h. An adsorption stoichiometry of Pt/CO of 1 was assumed to calculate the metal dispersion [28].

3. Results

3.1. Characterization of $Pt/Ba/CeO_2$ and $Pt/Ba/Al_2O_3$

XRD analysis of the fresh catalysts revealed in both cases the presence of crystalline $BaCO_3$ (not shown). The characteristic reflections of Pt or PtO_x were not observed due to the low amount of Pt in the catalyst and its high dispersion. The STEM images of the $Pt/Ba/Al_2O_3$ catalyst showed the formation of very small Pt particles with an average size below 5 nm (Fig. 1a). For the $Pt/Ba/CeO_2$ sample, the low contrast between Pt and CeO_2 in the HAADF images and also the small Pt particle size did not allow the determination of the size and spatial distribution of Pt on the catalyst surface (Fig. 1b).

The presence of a small amount of metallic Pt was found by XAS in the fresh $Pt/Ba/Al_2O_3$, whereas only oxidized Pt could be observed on the corresponding $Pt/Ba/CeO_2$ catalyst. The k^3-weighted Fourier-transformed EXAFS spectra (2.2–13.7 Å) taken at Pt L_3 edge (fluorescence mode) for Al_2O_3 and CeO_2 catalysts are depicted in Fig. 2. For comparison the FT-EXAFS spectra of a Pt foil and PtO_2 are also presented. In both catalysts the contribution of Pt–O at an *R*-value of 1.7 Å (not corrected for the phase shift) is prevalent. The formation of defined Pt–O–Ce bonds, as reported in references [9,29], which may inhibit the sintering of Pt could not be observed with the $Pt/Ba/CeO_2$ catalyst in these investigations.

The stability of Ba-containing species formed after catalyst preparation was verified by TPD-MS measurements performed during heating the samples with 10 °C/min in an inert atmosphere (He). The results are in agreement with a previous study [22] and revealed a higher stability of $BaCO_3$ when deposited on CeO_2 compared to Al_2O_3. The CO_2 evolution, recorded during thermal decomposition of $Pt/Ba/CeO_2$, started at 650 °C and exhibited three maxima (corresponding to the decomposition of the differently thermally stable phases of $BaCO_3$) up to 1125 °C. In contrast, $BaCO_3$ supported on Al_2O_3 decomposed at lower temperatures between 300 and 850 °C.

XPS-analysis uncovered some differences in the surface composition of the two catalysts (Table 1). The apparently higher concentration of Ba species observed for $Pt/Ba/CeO_2$ sample is caused by the higher molar mass of CeO_2 (molar ratios—$Pt/Ba/CeO_2$ 1:28:116; $Pt/Ba/Al_2O_3$ 1:28:196) and by the lower surface area of CeO_2 (95 m^2/g) compared to the Al_2O_3 (193 m^2/g) supported catalyst. For similar reason, the atomic surface concentration of Pt species should also be higher. Nevertheless the dispersion of Pt is similar on both catalysts suggesting a possible coverage of Pt particles by Ba-containing phases or CeO_2.

3.2. NO_x storage and reduction behavior of $Pt/Ba/Al_2O_3$, $Pt/Ba/CeO_2$, $Pt(1)\text{-top}/Ba/CeO_2$ and $Pt(4)\text{-top}/Ba/CeO_2$

The course of the NSR process was studied by Pulse TA–MS experiments at 300 °C. The thermogravimetric curves (TG) depicted in Fig. 3 uncover the mass uptake and mass loss recorded for Al_2O_3 and CeO_2 supported catalysts during NO_x storage and reduction of the stored NO_x, respectively. The observed mass changes during storage were the sum of two effects: $Ba(NO_3)_2$ formation and $BaCO_3$ decomposition while the mass loss during reduction resulted from the opposite reactions. The regeneration of the catalyst was done with 1 ml of propene after 1, 3 and 10 NO/O_2 cycles (each cycle consisted of 3 ml O_2 and 2 ml NO). This experimental procedure allowed the study of both the NO_x storage capacity and the effectiveness of the regeneration step after partial or complete consumption of the NO_x storage active sites.

Distinct differences in the NSR behavior of the $Pt/Ba/Al_2O_3$ and $Pt/Ba/CeO_2$ catalysts were observed during NO_x storage and reduction (regeneration) steps. The significantly higher dynamic NO_x storage capacity observed for the $Pt/Ba/Al_2O_3$ catalyst (mass uptake on the TG curve in Fig. 3) was accompanied with a complete reduction of the NO_x stored species formed after 1, 3 or 10 NO/O_2 cycles (mass loss). In contrast, the full regeneration of $Pt/Ba/CeO_2$ system could not be achieved after partial or complete NO_x saturation of the catalyst. These results are in agreement with the work of Theis et al. [20] concerning the catalyst regeneration.

The superior properties of $Pt/Ba/Al_2O_3$ in comparison with $Pt/Ba/CeO_2$ could be caused on the one side by the different textural properties of the two supports (surface area, pore volume) and on the other side by the different acidity of the supports which may lead to a different contact with Pt and formation of differently active Ba species [9,21].

The incomplete reduction of the stored NO_x species on $Pt/Ba/CeO_2$ catalysts leads to a slow decrease of their NO_x storage capacity with an increasing number of cycles. The remaining nitrate shell progressively grows and finally only a very small amount of Ba species will be active in the NSR process. Such behavior could be caused by several factors such as higher thermal stability of the stored NO_x species, partial covering of Pt particles by Ba species due to the lower surface area of CeO_2 (Pt was deposited first on the support) or the presence of Pt in oxidized form during catalyst regeneration (since metallic Pt is required for the reduction step).

To determine the difference between the thermal stability of the NO_x stored species formed on the two supports TPD experiments were performed with $Pt/Ba/CeO_2$ and $Pt/Ba/Al_2O_3$ catalysts after NO_x storage (Fig. 4a and b). Prior to decomposition both catalysts were exposed to 10 NO/O_2 cycles (not shown) to reach the maximum NO_x storage capacity (the mass uptake after subsequent NO/O_2 cycles did not change anymore). $Pt/Ba/Al_2O_3$ showed a slightly higher total storage capacity and captured the NO_x faster during the storage process than Pt/Ba/

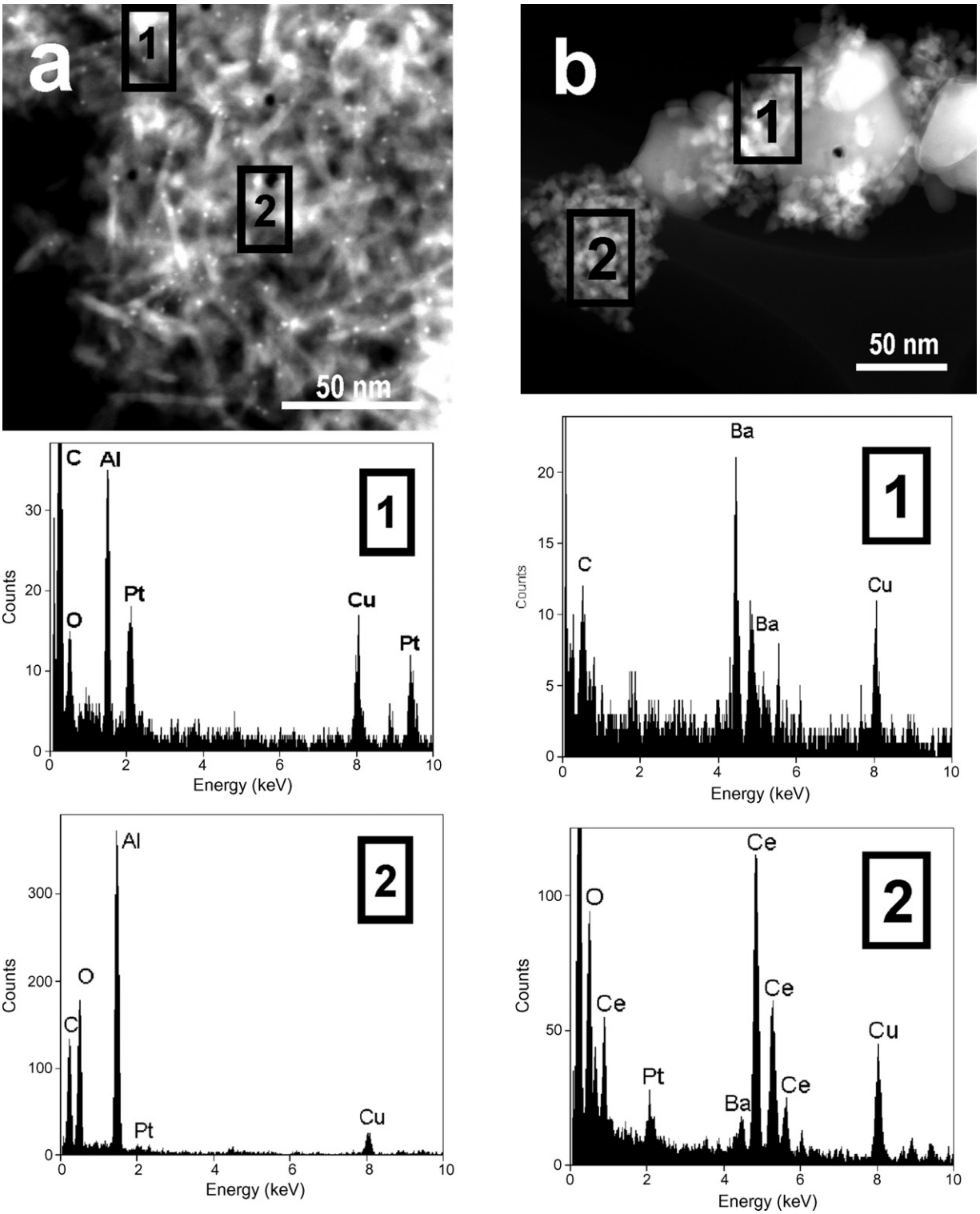

Fig. 1. STEM images of $Pt/Ba/Al_2O_3$ (a) and $Pt/Ba/CeO_2$ (b) with the EDX spectra obtained from the outlined regions depicted below.

CeO_2. The mass uptakes due to the NO_x storage for the alumina supported catalyst after 1, 3 and 10 NO/O_2 cycles amounted to 0.7, 1.56 and 2.45 mg, respectively, while the same amount of ceria-supported catalyst (70 mg) stored 0.45, 0.9 and 1.96 mg after 1, 3 and 10 NO/O_2 cycles, respectively. Moreover, for the alumina-supported catalyst the saturation by NO_x species was reached already after 6 NO/O_2 cycles, while for $Pt/Ba/CeO_2$ even 10 NO/O_2 cycles were not enough to reach saturation. The NO evolution observed by MS measurements during heating the samples in He with 10 °C/min uncovered the same temperature range for $Ba(NO_3)_2$ decomposition: ca. 300–700 °C. Nevertheless, the four regions of NO evolution observed for $Pt/Ba/CeO_2$ during TPD reveal the formation of $Ba(NO_3)_2$ phases with different thermal stability, as also described by Piacentini et al.

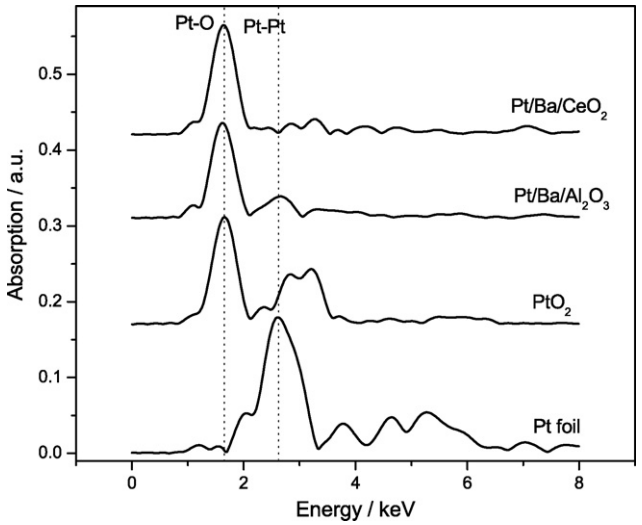

Fig. 2. Fourier transformed EXAFS data (k^3-weighted) at the Pt L_3 edge of fresh $Pt/Ba/CeO_2$ and $Pt/Ba/Al_2O_3$ catalysts.

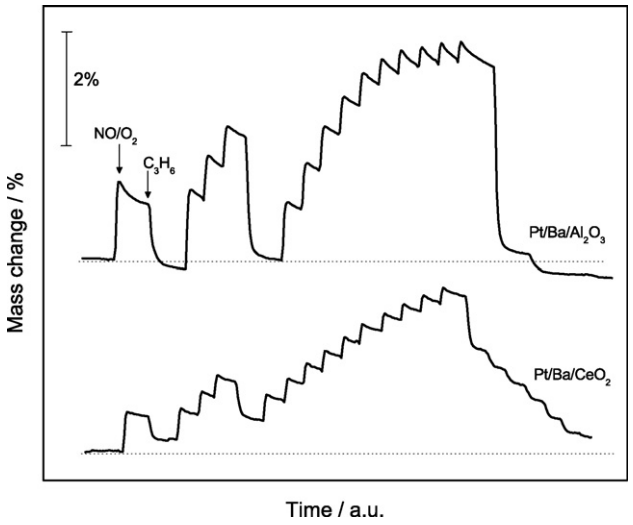

Fig. 3. Comparison of NSR activity at 300 °C for $Pt/Ba/CeO_2$ and $Pt/Ba/Al_2O_3$; observed mass gains result from the NO/O_2 pulses, mass losses from the pulses of C_3H_6.

[21]. The decomposition of $Ba(NO_3)_2$ formed on $Pt/Ba/Al_2O_3$ exhibited a maximum of the NO mass spectrometric signal at 483 °C, whereas on $Pt/Ba/CeO_2$ maxima appeared at 427, 519, 546 and at ca. 610 °C.

To check the effect of the possible coverage of Pt particle by Ba species during catalyst preparation, additional NSR experiments were performed using samples prepared by depositing first Ba species on CeO_2 followed by platinum. The TG curves recorded during NO_x storage and regeneration processes performed on the Pt(1)-top/Ba/CeO_2 and Pt(4)-top/Ba/CeO_2 samples are depicted in Fig. 5. For comparison Fig. 5 presents also the curve of the NSR evolution for the conventionally prepared $Pt/Ba/CeO_2$. The results obtained for Pt(1)-top/Ba/CeO_2 show a similar NO_x storage-reduction behavior as that observed for $Pt/Ba/CeO_2$. However, the amount of the stored NO_x species reduced by C_3H_6 was even slightly lower than that of the conventional catalyst. The reduction of stored NO_x species is improved by increasing the Pt content (see top curve in Fig. 5). One millilitre of C_3H_6 lead to the removal of 65% of the stored NO_x after 10 NO/O_2 cycles in Pt(4)-top/Ba/CeO_2, whereas only 28.5% of the stored NO_x was reduced in the Pt(1)-top/Ba/CeO_2 catalyst after 10 NO/O_2 cycles. Nevertheless, the improvement observed for the high loaded Pt sample could be caused by the formation of larger Pt particles which are less reoxidized during the NO_x storage process.

3.3. Decomposition of PtO_x

Two types of impregnated samples were used for investigating the thermal stability of alumina- and ceria-supported PtO_x: the high loaded 10-Pt/support and the low loaded Pt/Ba/support samples. TA–MS techniques were used to study the PtO_x decomposition on the high loaded 10-Pt/support samples while for the low loaded Pt/Ba/support catalysts *in situ* fluorescence XAS measurements were performed.

In Figs. 6a and b the results of TA–MS experiments on 10-Pt/Al_2O_3 and 10-Pt/CeO_2 samples are presented. The observed mass losses (TG curve) resulted from the decomposition of PtO_x which was, however, superimposed by the evolution of water and traces of CO_2 present in the fresh catalyst. Therefore the investigation of the stability of PtO_x was based on the mass spectrometric signal of evolved oxygen ($m/z = 32$). The O_2 evolution indicates the decomposition of PtO_x deposited on CeO_2 in the range of 150–815 °C and has three maxima which correspond to the decomposition of PtO_x species with different thermal stability, depending on the dispersion and intimate contact with the CeO_2 support. The corresponding data for 10-Pt/Al_2O_3 indicate that a higher temperature is necessary for PtO_x decomposition on alumina (ca. 325–960 °C). The $m/z = 32$ signal shows a maximum at ca. 600 °C.

PulseTA was used for the quantification of the O_2 evolved during decomposition of PtO_x deposited on CeO_2 or Al_2O_3. The data obtained uncovered a significant difference of the amount of O_2 evolved during decomposition. The values of x in formula PtO_x are 1.41 and 0.76 for alumina- and ceria-supported samples, respectively.

The *in situ* XAS measurements were performed on the corresponding 1% Pt samples during heating in Ar with 5 °C/min. The spectra were taken every 5 min and the

Table 1
Surface composition of $Pt/Ba/Al_2O_3$ and $Pt/Ba/CeO_2$ catalysts determined by XPS

Catalyst	Pt $4d_{5/2}$		Pt $4f_{7/2}$		O 1s		Al 2s		Ce $3d_{5/2}$		Ba $3d_{3/2}$		C 1s	
	at.%	E_b (eV)	at.%	E_b (eV)	at.%	E_b (eV)	at.%	E_b (eV)	at.%	E_b (eV)	at.%	E_b (eV)	at.%	E_b (eV)
$Pt/Ba/Al_2O_3$	0.1	316.8	–	–	71.1	531.6	21.4	119.4	–	–	5.6	796.2	1.8	289.4
$Pt/Ba/CeO_2$	–	–	0.1	72.0	52.1	530.7	–	–	13.9	881.6	25.9	795	8.0	289.4

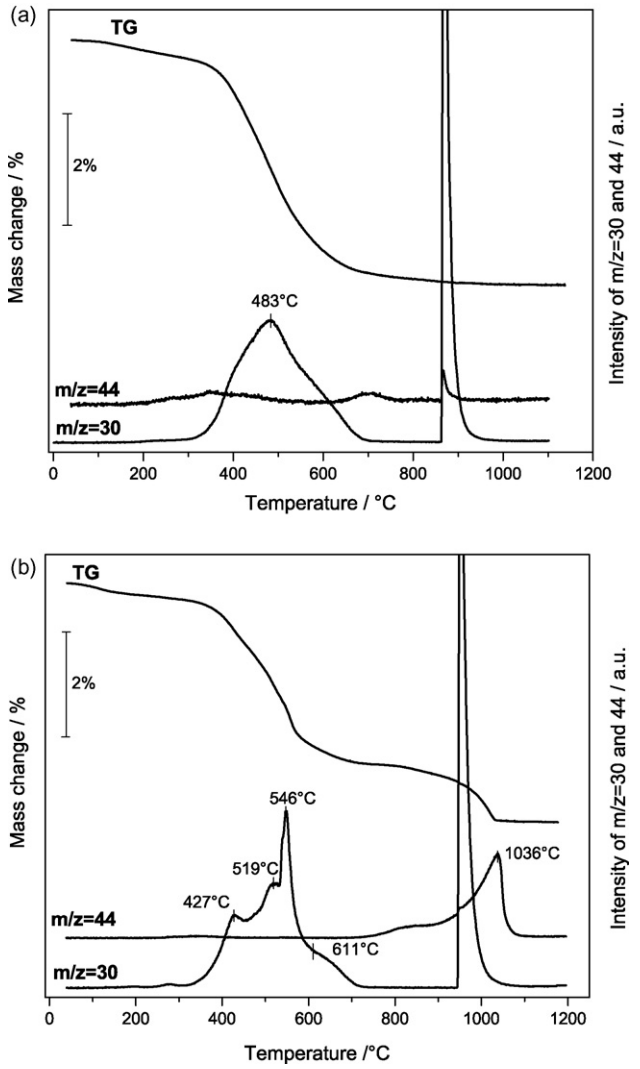

Fig. 4. Thermal analysis of $Pt/Ba/Al_2O_3$ (a) and $Pt/Ba/CeO_2$ (b) after complete saturation of NO_x storage sites. The amount of stored NO_x ($m/z = 30$) was quantified by injecting of 1 ml NO pulse at the end of each experiment.

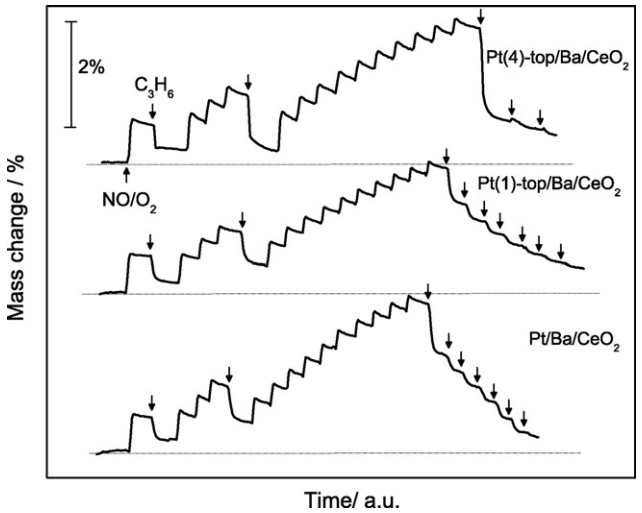

Fig. 5. NO_x storage-reduction activity at 300 °C of $Pt(1)\text{-top}/Ba/CeO_2$ and $Pt(4)\text{-top}/Ba/CeO_2$ compared with the $Pt/Ba/CeO_2$ catalyst.

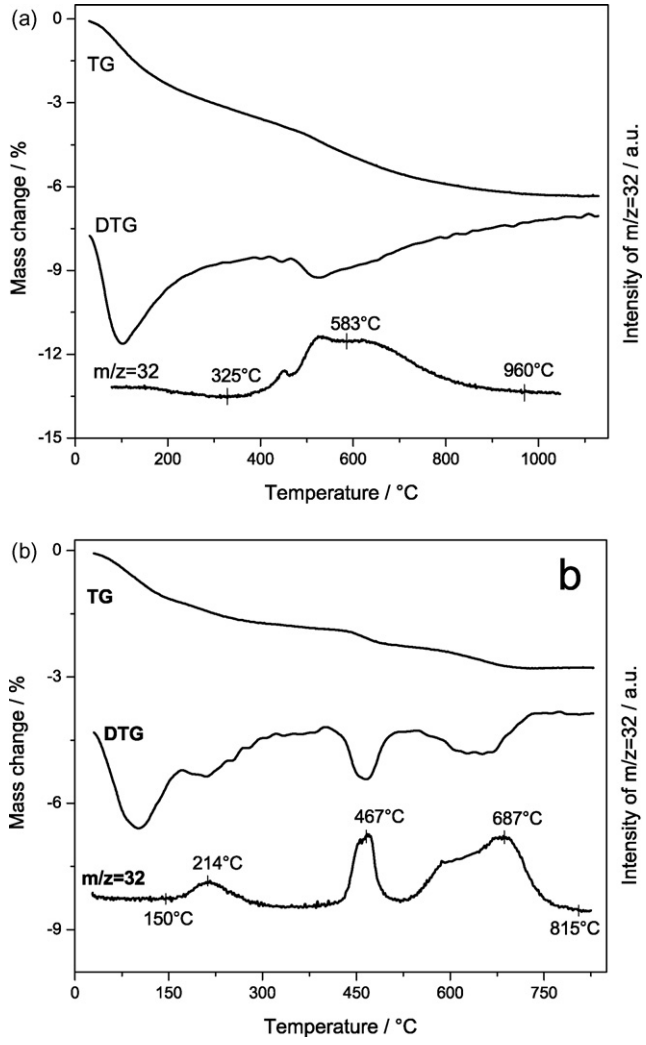

Fig. 6. TG, DTG and O_2 ($m/z = 32$) mass spectrometric signal recorded during decomposition of PtO_x in $Pt(10)/Al_2O_3$ (a) and $Pt(10)/CeO_2$ (b).

corresponding results of the $Pt/Ba/Al_2O_3$ and $Pt/Ba/CeO_2$ catalyst are shown in Fig. 7a and b. The XANES spectrum of Pt foil is presented for comparison. The absorption intensity of the white line in the case of Pt L_3 edge reflects the vacancy in the 5d orbital of Pt (electron transition from 2p to 5d) and is therefore related to the oxidation state. Thus the decrease of the white line intensity indicates a continuous reduction of Pt from high oxidation (Pt^{4+} or Pt^{2+}) to metallic state. In $Pt/Ba/Al_2O_3$ platinum was reduced at ca. 450 °C while on corresponding ceria-supported samples the decomposition of PtO_x occurred faster and was finished already at 370 °C. These results are in line with the TA–MS data presented above which indicate that PtO_x on CeO_2 releases oxygen at lower temperature than on Al_2O_3.

3.4. Pre-reduction treatment of $Pt/Ba/CeO_2$ catalyst and its influence on the NSR performances

The NO_x storage and reduction behavior of pre-reduced $Pt/Ba/CeO_2$ samples was measured and compared to that of the fresh $Pt/Ba/CeO_2$ catalyst. Each sample was kept under He

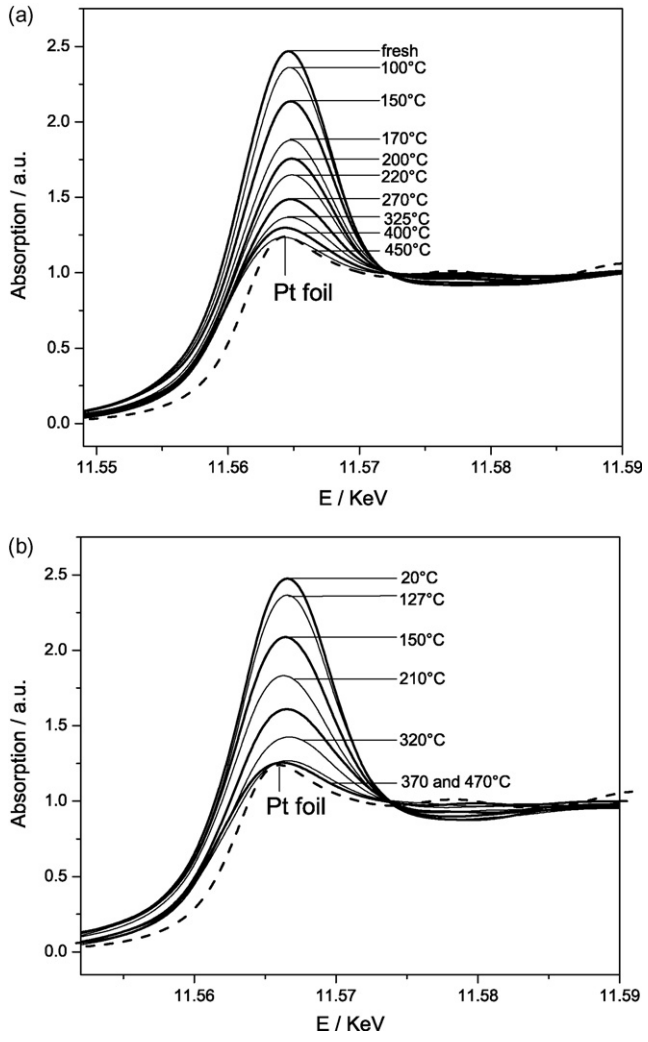

Fig. 7. *In situ* XAS investigation of the Pt L_3 edge during PtO_x decomposition in $Pt/Ba/Al_2O_3$ (a) and $Pt/Ba/CeO_2$ (b) while heating with 5 °C/min in Ar.

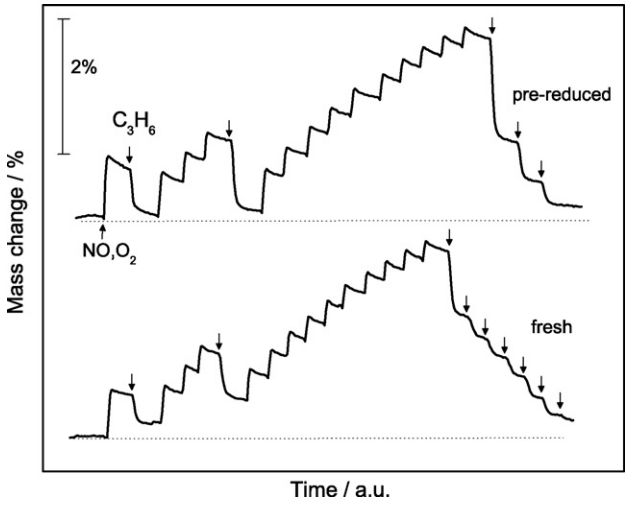

Fig. 8. Influence of the pre-reduction treatment at 500 °C on the NO_x storage and reduction behavior of $Pt/Ba/CeO_2$ at 300 °C. Mass gains results from the NO/O_2 and mass losses are due to C_3H_6 pulses.

(50 ml/min) at the pre-reduction temperature (300, 400, 500, 600 or 700 °C) for 45 min and reduced by four 1 ml H_2 pulses. After pre-reduction the NSR processes were monitored at 300 °C.

Fig. 8 shows the NO_x storage-reduction behavior of the $Pt/Ba/CeO_2$ catalyst before and after the pre-reduction treatment at 500 °C. The reduction of the catalyst before NSR has a beneficial effect on the storage and, especially, on the reduction (regeneration) activity. The influence of pre-reduction temperature on the NSR performance is summarized in Fig. 9b.

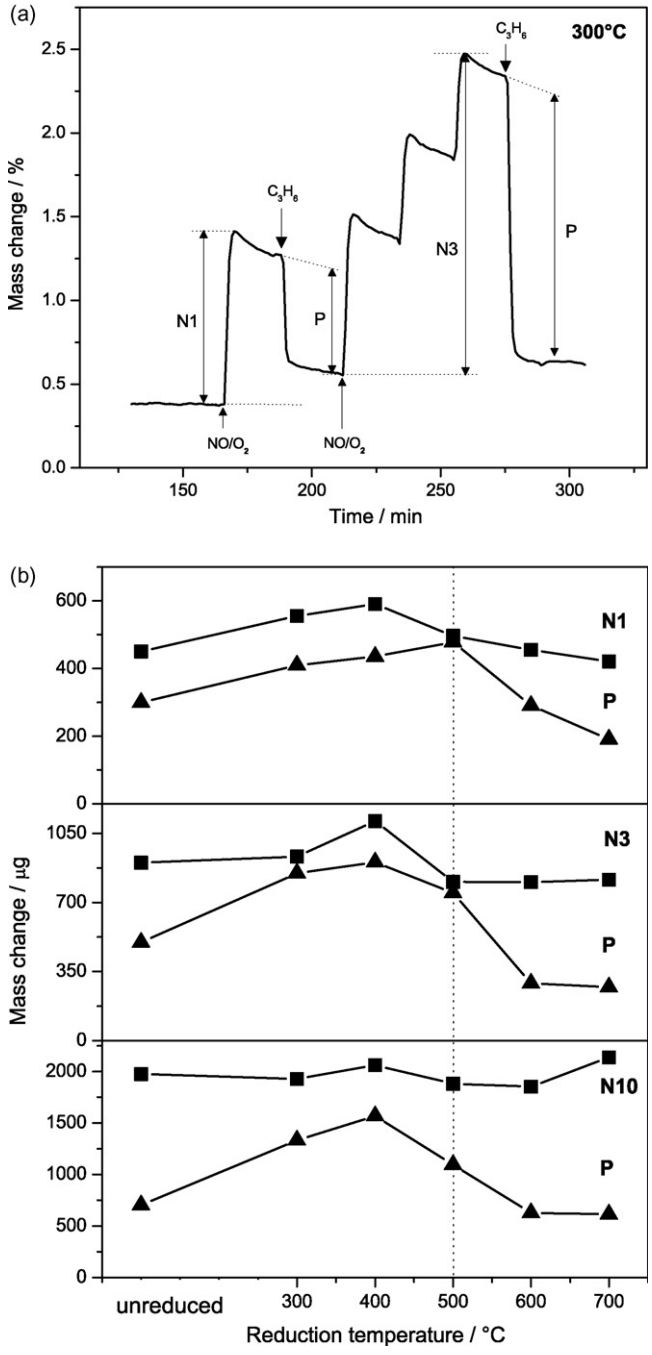

Fig. 9. (a) Determination of the amount of stored NO_x after one (N_1), three (N_3) and ten (N_{10}, not shown) pulses. The amount of reduced NO_x resulting from one pulse of C_3H_6 is denoted as P. (b) Influence of the pre-reduction temperature on the amount of stored and reduced NO_x.

Quantification of the stored NO_x (after 1, 3 and 10 NO/O_2 cycles—denoted as N1, N3 and N10 in Fig. 9) and of the NO_x reduced by 1 ml of propene (denoted as P) was achieved by monitoring the mass changes in TG measurements. Due to the high temporary concentration of NO immediately after the pulse injection the equilibrium of NO oxidation is shifted towards NO_2 formation. Thus, the influence of pre-reduction on the activity of the Pt for the oxidation of NO to NO_2 and consequently on the NO_x storage process could not be observed. The exposure of the $Pt/Ba/CeO_2$ catalyst to the H_2 containing atmosphere beneficially influenced the regeneration activity of the catalyst in the temperature range of 300–500 °C, whereas at higher temperature (600–700 °C) the activity significantly decreases. Five hundred degree Celsius seems to be the most suitable temperature for the pre-reduction, the catalyst reduced at this temperature is completely regenerated by 1 ml of C_3H_6 after exposure to 1 or 3 NO/O_2 cycles. This is an important observation because the active sites for NO_x storage are only partially consumed during the real technical application (switch from lean to reach occurs before NO_x saturation is reached).

In order to check if the enhanced regeneration activity of the pre-reduced $Pt/Ba/CeO_2$ catalyst is stable when NSR cycles are repeated the sample was exposed to alternate lean-rich cycles for 8 h. The results indicate that the activity of the catalyst was constant over the time scale of these experiments (not shown).

Exposure of the sample to 500 °C before the experiment resulted in the decomposition of PtO_x on both CeO_2 and Al_2O_3 supports and consequently only metallic Pt was present in catalysts at the beginning of the NO_x storage-reduction cycle. This behavior was confirmed by XAS analysis (Fig. 7). Thus, in order to check which of the two factors, i.e. the presence of hydrogen or exposure to high temperatures (or both) exert the main influence on the NO_x reduction activity of $Pt/Ba/CeO_2$, the sample was aged under inert atmosphere (He) at 500 °C for 45 min. The results did not show any improvement of the activity after this treatment (not shown), indicating that heating alone is not effective.

3.5. Effect of H_2 reducing atmosphere on the catalyst properties

3.5.1. Effect on platinum particle size

The change in Pt particle size after exposure to reducing atmosphere was investigated by electron microscopy. Due to very small Pt particles and little contrast between platinum and ceria, it was impossible to investigate the CeO_2 supported samples with low Pt loading. Therefore, a sample with a higher loading of platinum, $4\text{-}Pt/CeO_2$, was prepared and pre-reduced at 400, 600 and 1000 °C. All samples were exposed to air before measurements. The STEM images of pre-reduced $4\text{-}Pt/CeO_2$ revealed a slight sintering of Pt and CeO_2 particles after 45 min pre-reduction at high temperatures (Fig. 10) but the average particle size did not exceed 10 nm after exposure to 1000 °C under reducing atmosphere. EDX analysis at some selected points did not show any indication of Ce–Pt alloy [30] formation at 1000 °C.

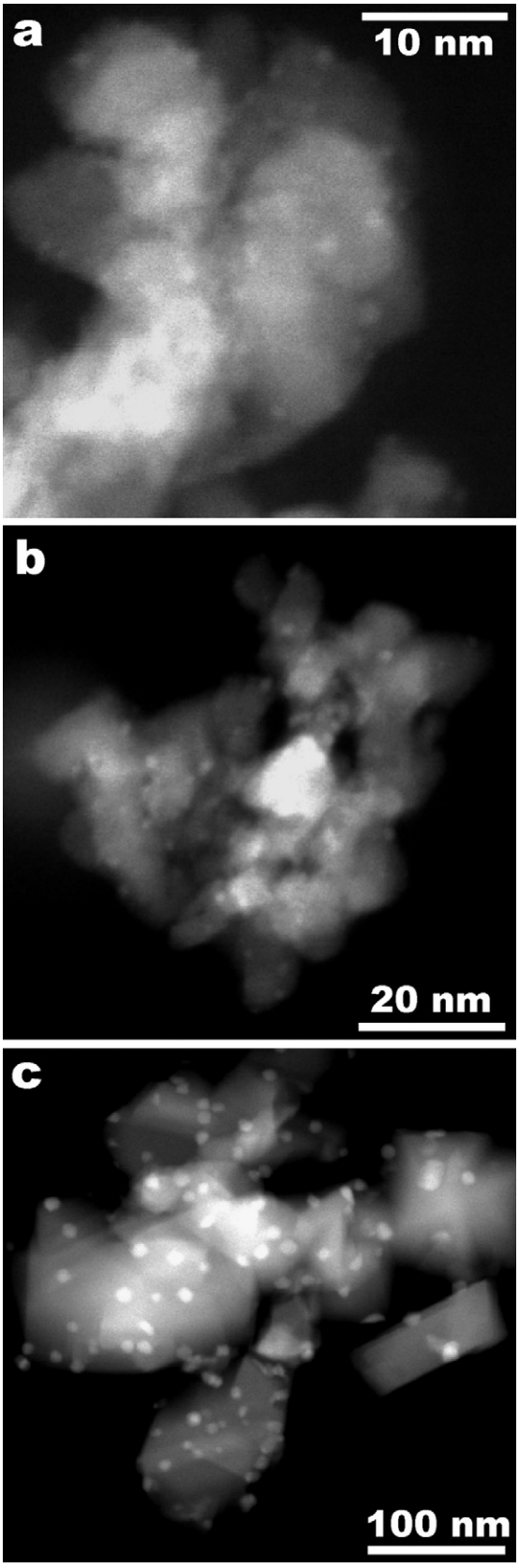

Fig. 10. STEM images of $4\text{-}Pt/CeO_2$ after pre-reduction with four 1 ml pulses of H_2 at 400 °C (a), 600 °C (b) and 1000 °C (c).

CO chemisorption measurements on the Pt/Ba/CeO_2 catalyst revealed a significant decrease of Pt chemisorption capacity with increasing reduction temperature in pure H_2. The molar ratio of CO/Pt dropped from 0.97 (reduced at 500 °C) to 0.31 after reduction at 700 °C for 1 h. Due to the fact that CeO_2 may also chemisorb large amounts of CO [31,32] and some sintering and reduction of CeO_2 in pure H_2 was observed at higher temperature [33] these values hint towards sintering or, possibly, the migration of CeO_2 on top of the metal particle surface [4,30].

Additional XAS measurements at Pt L_3 edge corroborated these results. The Pt/Ba/CeO_2 catalyst was pre-reduced in the thermoanalyzer at different temperatures in the range of 300–950 °C. Since the samples were exposed to air before the synchrotron experiments, the XANES spectra at Pt L_3 edge show a gradual reoxidation of Pt particles. The results indicate that a higher pre-reduction temperature and thus increased Pt particles size results in a decrease of the extent of Pt reoxidation after exposure to air at ambient temperature (Fig. 11). All these results support the conclusion that the pre-reduction at 500 °C leads to mild sintering, while the exposure to H_2 at 950 °C results in more severe sintering of Pt particles.

The local structure of Pt in the pre-reduced Pt/Ba/CeO_2 sample was analyzed by EXAFS and compared to that obtained for the sample aged in Ar. The Fourier transformed k^3-weighted EXAFS spectra taken at room temperature for Pt/Ba/CeO_2 after 45 min in 5% H_2/He atmosphere at 500 °C show a lower back-scattering contribution typical for Pt–O bond and a stronger contribution of Pt-backscatter than the sample aged in Ar at the same temperature (not shown).

3.5.2. Textural properties

The BET surface area and the pore volume measured for Pt/Ba/CeO_2 after ageing under reducing atmosphere (4 ml H_2 pulses in 50 ml/min He) at 500, 600 and 700 °C for 45 min did not show any significant changes compared to that of the fresh sample (55 m^2/g fresh material and 52 m^2/g after ageing at 700 °C). Thus, the mild reduction condition applied in our investigation did not lead to a decrease in CeO_2 surface area as observed, e.g. by Perrichon et al. [33] during exposure to pure H_2 above 550 °C. This may also be due to the different stability of the CeO_2 used during this study.

3.5.3. Cracking of C_3H_6 on Pt/Ba/Al_2O_3 and Pt/Ba/CeO_2 after pre-reduction

The Pt/Ba/support samples, fresh and pre-reduced at 500 and 700 °C (by 4 ml of H_2), were selected to study the cracking of C_3H_6 at 300, 400 and 500 °C by PulseTA. The catalysts were heated to 500 °C for surface cleaning and then cooled to 300 °C. Before the experiment 2 ml O_2 were injected to simulate the oxidation state of Pt at the reaction temperature under real conditions before C_3H_6 pulses. Pulses of 1 ml C_3H_6 and 1 ml O_2 were injected alternatively to the sample and the evolving gases were monitored by MS. Using the same sample the procedure was repeated at 400 and 500 °C. The yield of propene cracking was estimated by quantification of the H_2 evolved during experiments and the results are presented in Fig. 12. The *Y* axis shows (in percent) the ratio of the hydrogen evolved related to the total amount of hydrogen present in 1 ml propene. For both catalysts the extent of C_3H_6 dissociation increases with higher reaction temperature. Nevertheless, due to the higher dispersion of Pt particles on CeO_2 the efficiency of the process is higher above 400 °C on Pt/Ba/CeO_2. Interestingly, the pre-reduction treatment does not influence the catalytic activity of Pt particles in Pt/Ba/Al_2O_3 but affects the activity of Pt/Ba/CeO_2. The amount of cracked C_3H_6 decreases significantly after pre-reduction of the ceria-supported catalyst at 700 °C.

3.5.4. Redox properties Pt/CeO_2 at different temperatures

The conventional TPR experiments (carried out in reducing atmosphere) offer only an integral view on the Pt/CeO_2 redox behavior and consequently the amount of oxygen which can be removed by reduction of CeO_2 to Ce_2O_3 was measured by PulseTA experiments under isothermal conditions between 100 and 900 °C. The BET surface area of the Pt/CeO_2 sample used for these measurements was 85 m^2/g. Before experiments the

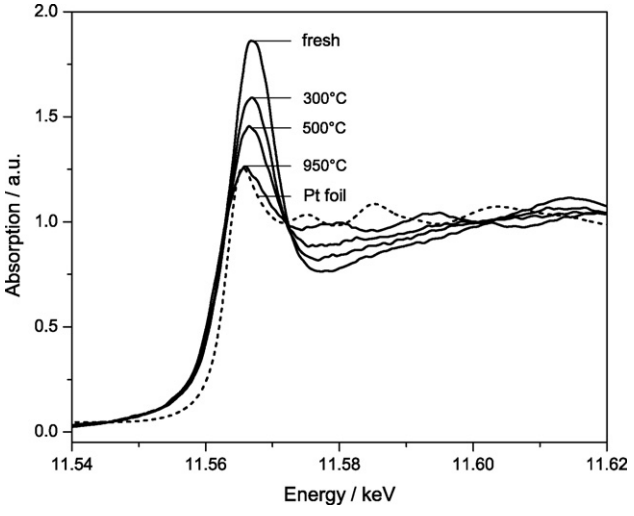

Fig. 11. Fluorescence XANES spectra taken at the Pt L_3 edge for Pt/Ba/CeO_2 after pre-reduction at different temperatures and exposure to air at 25 °C.

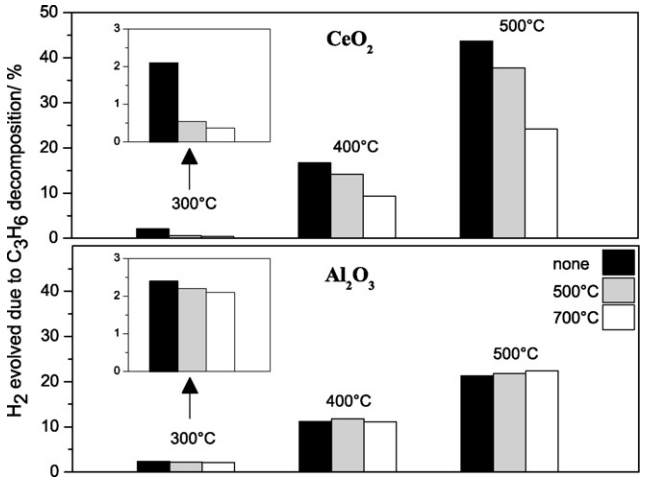

Fig. 12. Influence of the pre-reduction temperature (none, 500 and 700 °C) on the yield of propene cracking on Pt/Ba/CeO_2 and Pt/Ba/Al_2O_3 at 300, 400 and 500 °C.

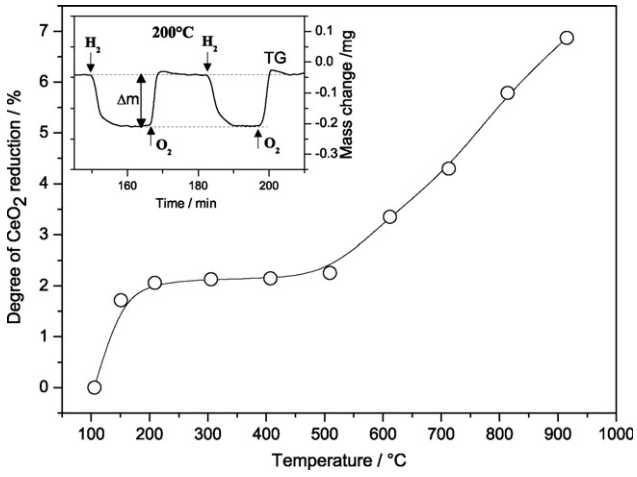

Fig. 13. Reduction degree of CeO_2 as a function of the temperature. The inset presents the mass changes recorded at 200 °C resulting from the alternative 2 ml pulses of H_2 and O_2.

samples were heated in He to 500 °C for removal of H_2O and adsorbed species. In a next step, two pulses of 1 ml of O_2 were injected over the sample for achieving total oxidation of the ceria at the reaction temperature. Then H_2 (2 ml) and O_2 (2 ml) pulses were alternatively injected into He carrier gas every 20 min. The mass uptake and mass loss recorded during reduction and reoxidation at 200 °C are shown in the inset of Fig. 13 and illustrate the method applied for quantification of the removed oxygen. The shape of the TG curve indicates a very fast reduction and reoxidation of CeO_2. The CeO_2 reduction degree (calculated as the ratio of removed oxygen to the total amount of oxygen removed during reduction of Ce^{4+} to Ce^{3+}) as a function of temperature is shown in Fig. 13. The results indicate reduction of surface CeO_2 at lower temperature and bulk reduction at higher temperature, as observed also in other studies [4,11,34]. The reduction of the outer layers of the CeO_2 used during this study starts already at 150 °C. The amount of the removed oxygen at 200 °C amounts to ca. 2% of the whole removable oxygen. Between 200 and 500 °C no increase of this amount is observed. Above 500 °C a further increase of the amount of reducible oxygen indicates the beginning of the bulk ceria reduction.

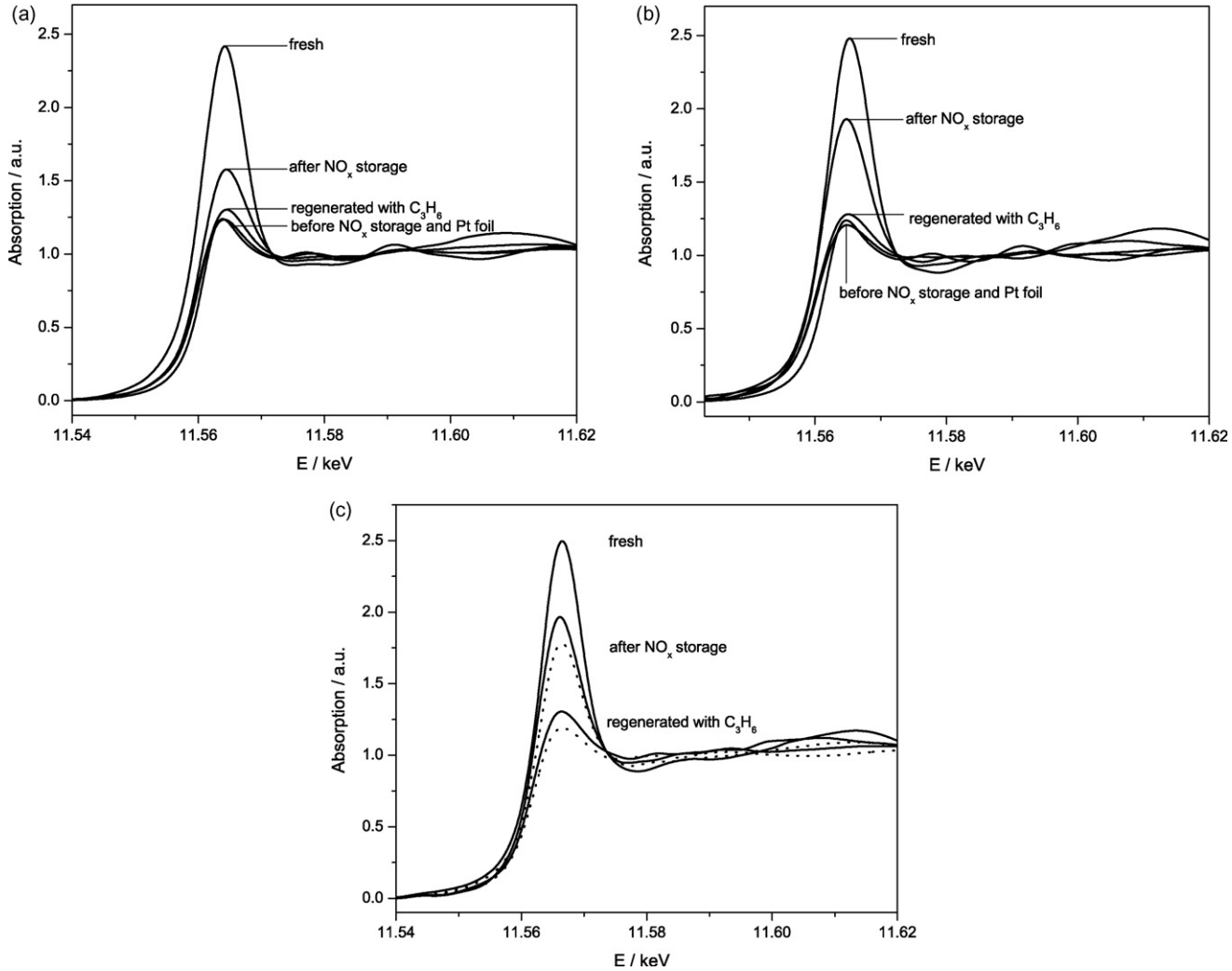

Fig. 14. *In situ* XAS measurements at the Pt L_3 edge during the NO_x storage and reduction processes on $Pt/Ba/Al_2O_3$ (a) and $Pt/Ba/CeO_2$ (b). Comparison of the height of the white-lines corresponding to pre-reduced and fresh $Pt/Ba/CeO_2$ sample before reaction, after NO_x storage and after catalyst regeneration with C_3H_6 (c).

3.6. Change in Pt oxidation state during NO_x storage-reduction processes on $Pt/Ba/Al_2O_3$ and $Pt/Ba/CeO_2$

In order to monitor element specifically the oxidation state of Pt during the storage and reduction process, *in situ* XAS measurements at the Pt L_3 edge were performed using a spectroscopic cell which allows the analysis of the samples by fluorescence EXAFS, transmission EXAFS, and XRD [35]. While transmission and fluorescence data were used for the analysis of $Pt/Ba/Al_2O_3$, for $Pt/Ba/CeO_2$ due to the high concentration of elements such as Ce and Ba in this sample, which strongly absorb the X-rays, only fluorescence data were processed. The fresh samples were first heated with 5 °C/min in 50 ml/min Ar to 500 °C for surface cleaning. Then the samples were cooled to 300 °C and exposed for 30 min to a NO–O_2–He gaseous mixture to simulate the lean period and, afterwards, the regeneration (reduction) of the catalyst was performed with a gaseous mixture of C_3H_6–He (30 min) corresponding to the rich period. The change of the oxidation state of Pt in the two catalysts during NSR lean-rich cycle was followed by recording XANES spectra every 5 min. Fig. 14a and b show the normalized spectra of catalysts taken at room temperature (fresh), at 300 °C before and after NO_x storage and after regeneration with C_3H_6. The XANES spectra of Pt foil is also shown as a reference. In both cases, Al_2O_3- and CeO_2-supported catalysts, PtO_x decomposed during heating to 500 °C in inert atmosphere and platinum was in metallic state at the beginning of the NO_x storage-reduction process. However, during the lean-rich cycles the reoxidation (the difference between the white-line peak height of the oxidized Pt and Pt foil) and then the reduction of Pt (during catalyst regeneration) were different for $Pt/Ba/Al_2O_3$ and $Pt/Ba/CeO_2$. The lower extent of oxidation of Pt after 30 min exposure to NO/O_2 oxidizing atmosphere suggests for $Pt/Ba/Al_2O_3$ the presence of larger Pt particles which could be oxidized only at the surface (Pt passivation [36]). On the contrary, the smaller particle size of Pt in $Pt/Ba/CeO_2$ and the influence of the CeO_2 support lead to a more profound oxidation. The regeneration of the catalyst surface, which should at first cause the reduction of PtO_x seems also to be influenced by the size of the Pt particles. The time-resolved spectra (not shown) showed a gradual decrease of the Pt oxidation state for $Pt/Ba/CeO_2$ catalyst, while the reduction of Pt on Al_2O_3 occurred immediately.

In addition, the effect of the pre-reduction on the Pt redox behavior was studied by XAS for $Pt/Ba/CeO_2$. The sample was heated to 500 °C (5 °C/min) in Ar and then exposed to 5% H_2/He for 45 min at this temperature. Subsequently, the sample was cooled to 300 °C in Ar and subjected to NO–O_2–He and C_3H_6–He atmospheres. The difference between the white-line peak heights corresponding to pre-reduced and unreduced $Pt/Ba/CeO_2$ sample before reaction, after NO_x storage and after catalyst regeneration by C_3H_6 is shown in Fig. 14c. The results indicate that the larger Pt particles formed after pre-reduction with H_2 at 500 °C were less reoxidized during NO_x storage and faster reduced by C_3H_6.

4. Discussion

In this study the NO_x storage-reduction behavior of $Pt/Ba/CeO_2$ was investigated and compared to that of $Pt/Ba/Al_2O_3$. The results provide crucial information about the influence of the support on the NSR activity and based on these findings a possible pre-treatment is suggested for increasing the regeneration activity of $Pt/Ba/CeO_2$ under idealized conditions.

The study showed that the NO_x storage and, particularly, the regeneration activity are superior for the Al_2O_3 supported catalyst. The higher storage capacity of $Pt/Ba/Al_2O_3$ compared to $Pt/Ba/CeO_2$ may be explained by the influence of textural and chemical properties of the support. The lower surface area of CeO_2 and also a different interaction with the supported species lead to the formation of more stable $BaCO_3$ phases [37]. In addition, Pt particles may be covered during catalyst preparation by barium containing species or CeO_2. As a consequence, the oxidation of NO to NO_2 on the Pt surface and the formation of $Ba(NO_3)_2$ species may be hindered.

More relevant is the difference in the reduction of stored NO_x species on $Pt/Ba/Al_2O_3$ and $Pt/Ba/CeO_2$. Considering that during the rather complex regeneration step, where (i) the partial reduction of the support (CeO_2) may occur, (ii) the nitrates are decomposed and (iii) the migration of the NO_x to reduction sites occurs, (iv) the reduction agent is activated, and finally (v) NO_x is reduced to N_2 [38], a number of phenomena may affect the regeneration of the $Pt/Ba/CeO_2$ NSR catalyst.

The oxygen-storage capacity of CeO_2 leads to an increase of the amount of available oxygen at the catalyst surface compared to the Al_2O_3-supported catalyst. This mobile oxygen can partially react with the reducing agent and thereby decrease the regeneration extent when the reducing agent is limited (pulse type experiments). Nevertheless, the results presented in Section 3.5.4 showed that at 300 °C only ca. 2% of the total oxygen, which would be consumed by the reduction of Ce^{4+} to Ce^{3+}, reacts with H_2 (Fig. 12b). This corresponds to a mass loss smaller than 0.1% during the regeneration process (Fig. 3). Thus only a small amount of C_3H_6 will be consumed by this process. However, at higher temperatures the progress of CeO_2 reduction may increase as the reduction of bulk CeO_2 becomes possible (Fig. 12b).

TPD of $Pt/Ba/Al_2O_3$ and $Pt/Ba/CeO_2$ NO_x saturated catalysts indicated the formation of NO_x stored species in the form of barium nitrate which decompose in the same temperature range (ca. 300–700 °C) on both catalysts. Only a slightly higher thermal stability of $Ba(NO_3)_2$ phases on $Pt/Ba/CeO_2$ was observed compared to those on Al_2O_3 supported catalyst.

The possible partial coverage of Pt particles by Ba species or CeO_2, indicated by XPS measurements on the fresh $Pt/Ba/CeO_2$ catalyst, seems not to be the main origin for the lower regeneration activity. The NO_x storage-reduction activity of Pt(1)-top/Ba/CeO_2 catalyst did not increase upon deposition of Pt species on top of Ba/CeO_2. The improvement of the regeneration activity observed for Pt(4)-top/Ba/CeO_2 results from a higher number of active Pt sites or the formation of larger Pt particles which contain more metallic Pt, necessary for

NO_x reduction. But these results corroborate that platinum plays a key role and a closer examination of the process of NO_x reduction by hydrocarbons may allow some possible explanations.

Two types of mechanisms have been proposed in literature for NO_x reduction on selective catalytic reduction catalysts (SCR) and they are assumed to be relevant also for the reduction step in NSR catalysts [38]. The first one involves the dissociative adsorption of NO_x on reduced Pt sites. This leads to an oxidation of the sites which become inactive until they are reduced again by hydrocarbons [38–40]. In the second mechanism NO_x and the hydrocarbons react directly (e.g. Langmuir–Hinshelwood formalism) and the formation of surface intermediates such as nitro, nitrite, organic nitro or nitrite and isocyanate was observed [41,42]. The kinetic model of the NSR processes developed by Olsson et al. [43] based on the reduction pathway of Pt sites by C_3H_6 involves also the dissociative adsorption of C_3H_6 on Pt and formation of CH_x–Pt species which will directly participate in the reduction of NO. Even if not all the mechanisms require the intermediate reduction of Pt, most of the studies suggest that reduced Pt sites are necessary for efficient reduction of NO_x [38,44]. Moreover, the very small noble metal particles being faster oxidized were found to be less efficient than larger particles for both NO oxidation and NO_x reduction [45].

Higher dispersion of Pt particles on CeO_2 compared to that on Al_2O_3 supported catalyst was found during this study which is in line with previous investigations of CeO_2 containing systems [8,9,29]. Probably, the strong interaction between CeO_2 and Pt particles leads to the formation of the small Pt particles as evidenced by electron microscopy measurements (Fig. 1b) and indirectly emerges from the high reoxidation degree of Pt of the pre-reduced catalysts at room temperature (Fig. 7). Moreover, the amounts of metallic and oxidized platinum present in the ceria- and alumina- supported catalysts after preparation are different. The Fourier transforms of the Pt L_3 EXAFS spectra suggested that already in the fresh Pt/Ba/Al_2O_3 catalysts Pt exists in small amount as metallic Pt while only oxidized Pt could be found in Pt/Ba/CeO_2 (Fig. 2). According to Yoshida et al. the formation of platinum oxides is suppressed by a more acidic support [46]. The higher acidity of Al_2O_3 compared to that of CeO_2 [47], may thus lead to the formation of a smaller amount of PtO_x on the support surface during preparation and also during the use of the catalyst. The different interaction of platinum with the two supports was additionally indicated by the almost double amount of O_2 evolved during calcination of high loaded PtO_x/Al_2O_3 compared to that observed for PtO_x/CeO_2. Also, *in situ* XAS studies on the oxidation state of Pt during the NSR processes on the Pt/Ba/CeO_2 and Pt/Ba/Al_2O_3 reflected the different interaction with the support. The decomposition of PtO_x was observed below 500 °C for both systems but at lower temperature for the CeO_2 catalyst (Fig. 7—prior to each NSR experiment the sample was heated in He to 500 °C for surface cleaning and H_2O removal) and thus in both cases platinum was in reduced state before the NSR. However, a faster and more profound reoxidation of Pt particles was observed during the lean cycle for the ceria-supported catalyst (Fig. 14). This is in line with the fast reoxidation of Pt particles observed at room temperature for Pt/Ba/CeO_2 pre-reduced under mild conditions (Fig. 7). Besides, the complete reduction of PtO_x species by C_3H_6 during the catalyst regeneration step was only achieved for Pt/Ba/Al_2O_3. Thus the presence of highly dispersed Pt particles, which are faster reoxidized, seems to significantly influence the NO_x reduction process. This is in line with the findings reported in [45] where the very small noble metal particles were found to be less efficient than larger particles during NSR. These results appear to be controversial to the similar values of the yield of C_3H_6 cracking obtained at 300 °C (under inert atmosphere) for the two fresh catalysts (cf. Fig. 12). However, the NO_x reduction mechanism involves also, as described before, the dissociative absorption of NO_x on the Pt reduced sites and oxidation of the sites. The smaller Pt particles on the CeO_2 surface will be faster and stronger reoxidized and are therefore probably less active for a next NO_x dissociation step. As a result of this the catalyst regeneration efficiency of the fresh Pt/Ba/CeO_2 catalyst is significantly lower than that of the corresponding alumina supported sample.

Interestingly, our results demonstrate that the pre-reduction of the Pt/Ba/CeO_2 catalyst between 300 and 500 °C (Fig. 10) leads to an improvement of its regeneration activity while keeping its NO_x storage capacity. Considering the previous discussion, one may assume that this improvement is due to the growth of the Pt-particles. The electron microscopy and XANES/EXAFS data revealed a small increase of the Pt particle size after pre-reduction at temperatures below 500 °C. Additionally, at these low temperatures due to the strong interaction with the support the growth of Pt particles on ceria has been reported to occur in a well-defined manner [4], leading to cube–octahedrons truncated particles with facets like (1 1 1) and (0 0 1) planes. In fact, the thermal analysis data indicate some reduction of the ceria support (constant between 200 and 500 °C), which may lead to both: a changed metal-support interaction and sintering of Pt particles. The regeneration activity of the pre-reduced catalyst (500 °C) was constant even after 8 h of cyclic exposure to NO/O_2 and C_3H_6 containing atmospheres. This shows that a more durable Pt-based catalyst may be obtained [48], particularly in view of the different regeneration strategies reported [23].

Whereas below 500 °C the pre-reduction of the catalyst is beneficial for the regeneration activity, at higher pre-reduction temperatures the activity decreases even to lower values than those recorded for the fresh material (Fig. 10). Since the sintering of Pt particles is too low (cf. TEM and EXAFS data) to be considered as a reason for such a sudden decrease of the regeneration activity, the deactivation must have a different origin. Several groups [4,30,49–51] have reported that the reduction of Pt/CeO_2 at temperatures higher than 700 °C may cause the decoration of Pt particles by partially reduced CeO_2. Above 900 °C under pure hydrogen the formation of $CePt_5$ has been observed [30]. We observed a severe decrease of the CO chemisorption capacity of Pt/Ba/CeO_2 after reduction at 700 °C. Moreover, the amount of C_3H_6 cracked at 300 °C on Pt/Ba/CeO_2 surface decreased after catalyst pre-reduction at

700 °C compared to that obtain after pre-reduction at 500 °C (Fig. 13). In contrast there was no significant change in the C_3H_6 cracking activity of pre-reduced $Pt/Ba/Al_2O_3$. Finally, the more profound reduction of CeO_2 noticed above 500 °C (Fig. 12b) with decoration of Pt particles is in line with the observed deactivation. The exposure of the pre-reduced $Pt/Ba/CeO_2$ catalyst to oxidizing atmosphere during NO_x storage at 300 °C is not effective for recovering the undecorated Pt particles, more severe treatments are required [4].

The results show that the beneficial effect of stabilizing the metallic state of Pt particles by pre-reduction, which seems to be crucial for the regeneration step, is lost at higher temperatures. Hence, these model studies show that not only the nature of the support but also the pre-treatment conditions significantly influences the NSR-properties of $Pt/Ba/MeO_x$ catalysts.

5. Conclusion

The present study has provided further insight into the use of ceria as support in NSR catalysts. The experiments showed a superior NSR activity of as-prepared $Pt/Ba/Al_2O_3$ compared to that of corresponding CeO_2 catalysts. This could be traced back to a strong interaction between Pt particles and CeO_2 which leads to a high platinum dispersion and a rather high extent of re-oxidation during the NSR-process. If a pre-reduction treatment is applied in the range of 300–500 °C the Pt particle size can be increased in a controlled way, which significantly improves the regeneration (reduction) activity of $Pt/Ba/CeO_2$. Pre-treated catalysts contain Pt particles which are more resistant against reoxidation, which is particularly important for the regeneration step. At too high pre-reduction temperature (>500 °C) the activity significantly decreases due to the possible migration of reduced ceria causing probably decoration or encapsulation of the noble metal. Further investigations are presently pursued in our laboratories to improve the NSR activity of $Pt/Ba/CeO_2$ catalysts and to further study the influence of ceria and other support materials.

References

[1] M. Ozawa, J. Alloys Compd. 275–277 (1998) 886.
[2] J. Kaspar, P. Fornasiero, M. Graziani, Catal. Today 50 (1999) 285.
[3] S.I. Matsumoto, Catal. Today 90 (2004) 183.
[4] A. Trovarelli (Ed.), Catalysis by Ceria and Related Materials, Imperial College Press, London, 2002.
[5] S. Hilaire, X. Wang, T. Luo, R.J. Gorte, J. Wagner, Appl. Catal. A 215 (2001) 271.
[6] P. Panagiotopoulou, D.I. Kondarides, Catal. Today 112 (2006) 49.
[7] A. Haryanto, S. Fernando, N. Murali, S. Adhikari, Energy Fuels 19 (2005) 2098.
[8] J.Z. Shyu, K. Otto, J. Catal. 115 (1989) 16.
[9] Y. Nagai, T. Hirabayashi, K. Dohmae, N. Takagi, T. Minami, H. Shinjoh, S.I. Matsumoto, J. Catal. 242 (2006) 103.
[10] M. Ozawa, J. Alloys Compd. 408–412 (2006) 1090.
[11] B. Harrison, A.F. Diwell, C. Hallett, Platinum Met. Rev. 32 (1988) 73.
[12] Y.-F.Y. Yao, J. Catal. 87 (1984) 152.
[13] A. Setiabudi, J. Chen, G. Mul, M. Makkee, J.A. Moulijn, Appl. Catal. B 51 (2004) 9.
[14] A. Trovarelli, C. de Leitenburg, M. Boaro, G. Dolcetti, Catal. Today 50 (1999) 353.
[15] M. Haneda, T. Morita, Y. Nagao, Y. Kintaichi, H. Hamada, PCCP 3 (2001) 4696.
[16] S. Philipp, A. Drochner, J. Kunert, H. Vogel, J. Theis, E.S. Lox, Top. Catal. 30–31 (2004) 235.
[17] M. Symalla, A. Drochner, H. Vogel, S. Philipp, U. Göbel, W. Müller, Top. Catal. 42–43 (2007) 199.
[18] J.A. Rodriguez, T. Jirsak, S. Sambasivan, D. Fischer, A. Maiti, J. Chem. Phys. 112 (2000) 9929.
[19] L.F. Liotta, A. Macaluso, G.E. Arena, M. Livi, G. Centi, G. Deganello, Catal. Today 75 (2002) 439.
[20] J. Theis, J. Ura, C. Goralski, J. Hungwen, E. Thanasiu, Y. Graves, A. Takami, H. Yamada, S. Miyoshi, SAE Paper SP-1759, 2003, 23.
[21] M. Piacentini, M. Maciejewski, A. Baiker, Appl. Catal. 72 (2007) 105.
[22] M. Casapu, J.-D. Grunwaldt, M. Maciejewski, M. Wittrock, U. Göbel, A. Baiker, Appl. Catal. B 63 (2006) 232.
[23] M. Casapu, J.D. Grunwaldt, M. Maciejewski, A. Baiker, S. Eckhoff, U. Göbel, M. Wittrock, J. Catal. 251 (2007) 28.
[24] M. Casapu, J.-D. Grunwaldt, M. Maciejewski, A. Baiker, M. Wittrock, U. Göbel, S. Eckhoff, Top. Catal. 42–43 (2007) 3.
[25] M. Maciejewski, C.A. Muller, R. Tschan, W.D. Emmerich, A. Baiker, Thermochim. Acta 295 (1997) 167.
[26] D. Briggs, M.P. Seah, Practical Surface Analysis by Auger and X-ray Photoelectron Spectroscopy, Wiley, Chichester, 1983.
[27] T. Ressler, J. Synchrotron Rad. 5 (1998) 118.
[28] J.R. Anderson, Structure of Metallic Catalysts, Academic Press, London, 1975.
[29] S. Hosokawa, M. Taniguchi, K. Utani, H. Kanai, S. Imamura, Appl. Catal. 289 (2005) 115.
[30] S. Bernal, J.J. Calvino, J.M. Gatica, C. Larese, C. Lopez-Cartes, J.A. Perez-Omil, J. Catal. 169 (1997) 510.
[31] A. Bensalem, J.C. Muller, D. Tessier, F. Bozon-Verduraz, J. Chem. Soc., Faraday Trans. 92 (1996) 3233.
[32] C. Binet, A. Badri, M. Boutonnet-Kizling, J.C. Lavalley, J. Chem. Soc., Faraday Trans. 90 (1994) 1023.
[33] V. Perrichon, A. Laachir, C. Abouarnadasse, O. Touret, G. Blanchard, Appl. Catal. A 129 (1995) 69.
[34] H.C. Yao, Y.F.Y. Yao, J. Catal. 86 (1984) 254.
[35] S. Hannemann, M. Casapu, J.-D. Grunwaldt, P. Haider, P. Trussel, A. Baiker, E. Welter, J. Synchrotron Rad. 14 (2007) 345.
[36] R.W. McCabe, C. Wong, H.S. Woo, J. Catal. 114 (1988) 354.
[37] M. Piacentini, M. Maciejewski, A. Baiker, Appl. Catal. B. 66 (2006) 126.
[38] W.S. Epling, L.E. Campbell, A. Yezerets, N.W. Currier, J.E. Parks, Catal. Rev. 46 (2004) 163.
[39] R. Burch, P.J. Millington, A.P. Walker, Appl. Catal. B 4 (1994) 65.
[40] V.I. Parvulescu, P. Grange, B. Delmon, Catal. Today 46 (1998) 233.
[41] D.K. Captain, C. Mihut, J.A. Dumesic, M.D. Amiridis, Catal. Lett. 83 (2002) 109.
[42] H. Abdulhamid, J. Dawody, E. Fridell, M. Skoglundh, J. Catal. 244 (2006) 169.
[43] L. Olsson, E. Fridell, M. Skoglundh, B. Andersson, Catal. Today 73 (2002) 263.
[44] J. Kaspar, C. de Leitenburg, P. Fornasiero, A. Trovarelli, M. Graziani, J. Catal. 146 (1994) 136.
[45] A.R. Vaccaro, G. Mul, J. Perez-Ramirez, J.A. Moulijn, Appl. Catal. B 46 (2003) 687.
[46] H. Yoshida, Y. Yazawa, N. Takagi, A. Satsuma, T. Tanaka, S. Yoshida, T. Hattori, J. Synchrotron Rad. 6 (1999) 471.
[47] D. Martin, D. Duprez, J. Phys. Chem. 100 (1996) 9429.
[48] D.H. Kim, Y.-H. Chin, G.G. Muntean, A. Yezeretz, N.W. Currier, W.S. Epling, H.-Y. Chen, H. Hess, C.H.F. Peden, Ind. Eng. Chem. Res. 45 (2006) 8815.
[49] S. Bernal, M.A. Cauqui, G.A. Cifredo, J.M. Gatica, C. Larese, J.A. Perez Omil, Catal. Today 29 (1996) 77.
[50] S.E. Golunski, H.A. Hatcher, R.R. Rajaram, T.J. Truex, Appl. Catal. B 5 (1995) 367.
[51] S. Bernal, J.J. Calvino, M.A. Cauqui, J.M. Gatica, C. Larese, J.A. Perez Omil, J.M. Pintado, Catal. Today 50 (1999) 175.